Shock structure and magnetic-field generation associated with relativistic jets in unmagnetized pair plasma

Jacek Niemiec[*], Ken-Ichi Nishikawa[†], Philip E. Hardee[‡], Martin Pohl[§], Mikhail Medvedev[¶], Yosuke Mizuno[†], Bing Zhang[‖], Mitsuo Oka[†], Helen Sol[**] and Dieter H. Hartmann[††]

[*]*Institute of Nuclear Physics PAN, ul. Radzikowskiego 152, 31-342 Kraków, Poland*
[†]*Center for Space Plasma and Aeronomic Research, University of Alabama in Huntsville, NSSTC, 320 Sparkman Drive, Huntsville, AL 35805, USA*
[‡]*Department of Physics and Astronomy,University of Alabama, Tuscaloosa, AL 35487, USA*
[§]*Department of Physics and Astronomy, Iowa State University, Ames, IA 50011, USA*
[¶]*Department of Physics and Astronomy, University of Kansas, KS 66045, USA*
[‖]*Department of Physics and Astronomy, University of Nevada, Las Vegas, NV 89154, USA*
[**]*LUTH, Observatore de Paris-Meudon, 5 place Jules Jansen, 92195 Meudon Cedex, France*
[††]*Department of Physics and Astronomy, Clemson University, Clemson, SC 29634, USA*

Abstract. **Using 3D and 2.5D particle-in-cell simulations we investigate the shock structure, magnetic-field generation, and particle acceleration associated with an unmagnetized relativistic electron-positron jet propagating into an unmagnetized pair plasma. The simulations use long computational grids which allow us to study the complete dynamics of the system. We find for the first time a relativistic shock system comparable to the predicted magnetohydrodynamic shock structure consisting of leading and trailing shocks separated by a contact discontinuity. Strong electromagnetic fields resulting from the Weibel instability are generated in the trailing shock where jet matter is thermalized and decelerated. We analyze the formation and nonlinear development through saturation and dissipation of those fields and associated particle acceleration. In the AGN context the trailing shock corresponds to the jet shock at the head of a relativistic astrophysical jet. In the GRB context this trailing shock can be identified with the bow shock driven by relativistic ejecta. The strong electromagnetic field near the trailing shock provides the emission site for afterglow emission from GRBs and may correspond to the hot spot at the leading edge of AGN jets.**

Keywords**: relativistic shocks, particle acceleration, magnetic fields**

I. INTRODUCTION

Particle-in-cell (PIC) simulations can shed light on the microphysics within relativistic collisionless shocks. Recent PIC simulations confirm that a relativistic shock in weakly or non magnetized plasma is dominated by the Weibel instability ([21], [5], [12], [13], [14], [16], [18], [19], [20], [6], [3], [4]). The associated current filaments and magnetic fields (e.g. [8]) accelerate electrons and cosmic rays, which affect the pre-shock medium [9].

In this paper we present new three-dimensional simulation results for an electron-positron jet injected into an electron-positron plasma using a long simulation grid [15]. A leading and trailing shock system develops with strong electromagnetic fields accompanying the trailing shock. Similar results has been recently obtained by us with two-dimensional experiments, which justifies the use of 2.5D (2D3V) simulation to study the complete dynamics of the system using even longer grids. The presentation below is based mostly on the results of the 3D run ([15]). The results of the large-scale 2.5D simulations will be presented at the Conference.

II. SIMULATION SETUP

The code used in this study is an MPI-based parallel version of the relativistic electromagnetic particle (REMP) code TRISTAN ([2], [11]). The 3D simulations have been performed using a grid with $(L_{\rm x}, L_{\rm y}, L_{\rm z}) = (4005, 131, 131)$ cells and a total of ~ 1 billion particles (12 particles/cell/species for the ambient plasma). The electron skin depth, $\lambda_{\rm s} = c/\omega_{\rm pe} = 10.0\Delta$, where $\omega_{\rm pe} = (e^2 n_{\rm a}/\epsilon_0 m_{\rm e})^{1/2}$ is the electron plasma frequency and the electron Debye length $\lambda_{\rm D}$ is half of the cell size, Δ. This computational domain is six times longer than in our previous 3D simulations ([14], [16]). Two-dimensional simulations allow us to use much larger grids. 2.5D test runs using computational grids with $(L_{\rm x}, L_{\rm y}) = (4005, 505)$ and $(4005, 1005)$ cells show results which are in very good agreement with 3D simulation.

As in our previous work (e.g. [14]) the jet is injected in a plane across the computational grid located at $x = 25\Delta$ in order to eliminate effects associated with the boundary at $x = x_{\rm min}$. The jet-electron number density in the simulation reference frame is $0.676\ n_{\rm a}$, where $n_{\rm a}$ is the ambient electron density, and the jet Lorentz factor is $\gamma_j = 15$. Both the jet and the ambient plasma are assumed to be cold, and in their reference frames the electron/positron thermal velocity is $v_{\rm j,th} = 0.014\ c$ and $v_{\rm a,th} = 0.05\ c$ for the jet and ambient plasma, respectively, where c is the speed of light. Radiating

boundary conditions are used at $x = x_{\rm min}$ and $x = x_{\rm max}$ boundaries, and periodic boundary conditions apply on the transverse boundaries [2].

The jet makes contact with the ambient plasma at a 2D interface (1D for 2.5D simulations) spanning the computational domain. Here the formation and dynamics of a small portion of a much larger shock are studied in a spatial and temporal way that includes the spatial development of nonlinear saturation and dissipation from the injection point to the jet front defined by the fastest-moving jet particles.

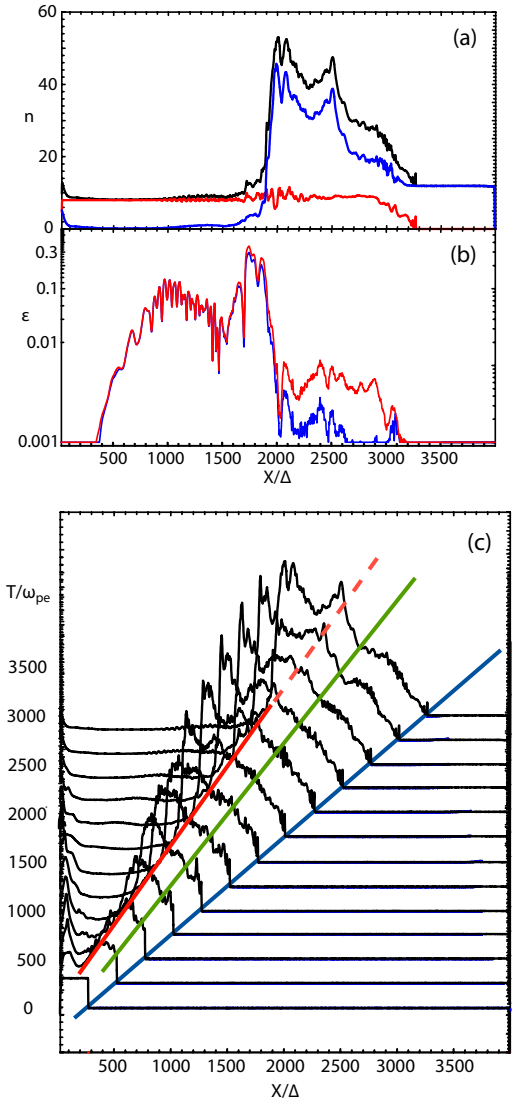

Fig. 1. Averaged values of (a): jet (red), ambient (blue), and total (black) electron density, and (b): electric (blue) and magnetic (red) field energy divided by the jet kinetic energy at $t = 3250\ \omega_{\rm pe}^{-1}$ for the 3D simulation. Panel (c) shows the evolution of the total electron density in time intervals of $\delta t = 250\ \omega_{\rm pe}^{-1}$. Diagonal lines indicate motion of the jet front (blue: $\lesssim c$), predicted contact discontinuity speed (green: $\sim 0.76\ c$), and trailing density jump (red: $\sim 0.56\ c$).

III. RESULTS

Figure 1a & b show the averaged (in the $y-z$ plane) (a) jet (red), ambient (blue), and total (black) electron density and (b) electromagnetic field energy divided by the total jet kinetic energy ($E_{\rm t}^{\rm j} = \sum_{i=e,p} m_{\rm i}c^2(\gamma_{\rm j}-1)$) at $t = 3250\ \omega_{\rm pe}^{-1}$ for the 3D experiment. Here, "e" and "p" denote electron and positron. Positron-density profiles are similar to electron profiles.

Ambient particles become swept up by the jet electrons and piled up at the front part of the jet. By $t = 3250\ \omega_{\rm pe}^{-1}$, the ambient-plasma density has evolved into a two-step plateau behind the jet front. The maximum density in this shocked region is about three times the initial density. The jet-plasma density remains nearly constant up to near the jet front.

Current filaments and strong electromagnetic fields accompany the growth of the Weibel instability in the trailing shock region. The electromagnetic fields are about four times larger than those seen previously using a much shorter grid system ($L_{\rm x} = 640\Delta$). At $t = 3250\ \omega_{\rm pe}^{-1}$, the electromagnetic fields are largest at $x/\Delta \sim 1700$, and decline by about one order of magnitude beyond $x/\Delta = 2300$ in the shocked region ([14], [16]).

Figure 1c shows the total electron density plotted at time intervals of $\delta t = 250\ \omega_{\rm pe}^{-1}$. The jet front propagates with the initial jet speed ($\lesssim c$). Sharp RMHD-simulation shock surfaces are not created (e.g. [10]). A leading shock region (linear density increase) moves with a speed between the fastest moving jet particles $\lesssim c$ and a predicted contact discontinuity speed of $\sim 0.76\ c$ (see section IV). A contact-discontinuity region consisting of mixed ambient and jet particles moves at a speed between $\sim 0.76\ c$ and the trailing density jump speed $\sim 0.56\ c$. A trailing shock region moves with speed $\lesssim 0.56\ c$. Note the modest density increase just behind the large trailing density jump.

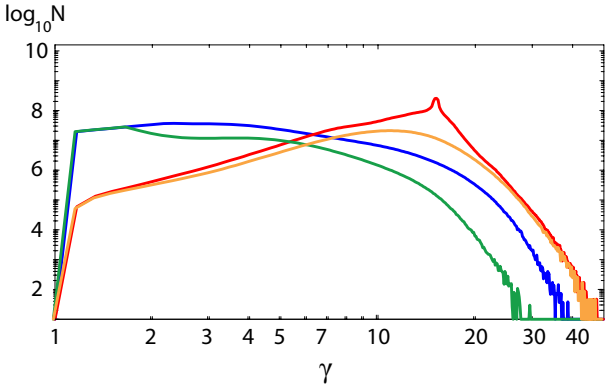

Fig. 2. Velocity distributions at $t = 3250\ \omega_{\rm pe}^{-1}$. All jet (red) and all ambient (blue), and at $x/\Delta > 2300$ jet (orange) and ambient (green) electrons are also plotted. The small (red) peak indicates jet electrons injected at $\gamma_j = 15$.

Figure 2 shows the velocity distribution of all jet (red) and ambient (blue) electrons in the simulation frame. The jet electrons injected with $\gamma_j = 15$ (note a small peak in red line in Fig. 2) become thermalized and accelerated to a non-thermal distribution due to Weibel instability-induced interactions. The swept-up

ambient electrons are heated by interaction with jet electrons. Some ambient electrons are also accelerated to speeds above the jet injection velocity. The velocity distributions of jet and ambient electrons near the jet front (at $x/\Delta > 2300$) are also plotted. The fastest jet electrons, $\gamma > 20$, are located near the jet front. On the other hand, the fastest ambient electrons are located farther behind the jet front (at $x/\Delta < 2300$). Thus, strong acceleration of the ambient electrons accompanies the strong fields associated with the Weibel instability.

IV. Discussion

Our collisionless-shock structure can be compared to 1-D hydrodynamic (**HD**) shock predictions (e.g. [1], [22]). The speed of the contact discontinuity (**CD**) is given by ram pressure balance in the CD frame. In the ambient frame that speed becomes ([17])

$$\beta_{\rm cd} = [(\gamma_{\rm j}\eta^{1/2})/(\gamma_{\rm j}\eta^{1/2}+1)]\beta_{\rm j}, \qquad (1)$$

where $\eta \equiv \rho_{\rm j}/\rho_{\rm a} = m_{\rm e}n_{\rm j}/m_{\rm e}n_{\rm a}$ and mass densities are determined in the "jet" and "ambient" proper frames. In our case $n_{\rm j} = 0.0451 n_{\rm a}$ and $\gamma_{\rm j} = 15$, and $\beta_{\rm cd} = 0.759$ ($\gamma_{\rm cd} = 1.54$) is the predicted CD speed. Formally this represents the average speed of particles in the CD region.

The leading shock moves at a speed given by

$$\gamma_{\rm ls}^2 = \frac{(\gamma_{\rm cd}+1)[\Gamma_{\rm sa}(\gamma_{\rm cd}-1)+1]^2}{\Gamma_{\rm sa}(2-\Gamma_{\rm sa})(\gamma_{\rm cd}-1)+2} \qquad (2)$$

where $5/3 > \Gamma_{\rm sa} > 4/3$ is the adiabatic index of the shocked ambient plasma. Thus the leading shock speed is predicted to be $0.865 > \beta_{\rm ls} > 0.783$ ($2 > \gamma_{\rm ls} > 1.6$) where upper and lower limits correspond to upper and lower limits of $\Gamma_{\rm sa}$, respectively.

The jump condition at the leading shock is

$$\frac{n_{\rm sa}}{n_{\rm a}} = \frac{\Gamma_{\rm sa}\gamma_{\rm cd}+1}{\Gamma_{\rm sa}-1}, \qquad (3)$$

where $n_{\rm sa}$ is the shocked ambient-plasma density in the proper (CD) frame, and we find $5.34\ n_{\rm a} < n_{\rm sa} < 9.15\ n_a$, where the lower and upper limits correspond to the upper and lower limits to $\Gamma_{\rm sa}$, respectively. Measured in the ambient (simulation) frame, the shocked ambient-plasma density should be $8.2\ n_{\rm a} < \gamma_{\rm cd} n_{\rm sa} < 14.1\ n_{\rm a}$. Formally this should represent the total density of particles in the shocked-ambient region.

Analogous computations for the trailing shock (see [15]) give the trailing-shock speed in the ambient (simulation) frame $0.35 < \beta_{\rm ts} < 0.61$, where the lower and upper limits correspond to adiabatic indices $\Gamma_{\rm sj} = 5/3$ and $\Gamma_{\rm sj} = 4/3$ of the shocked jet plasma. The proper density of shocked jet material is $0.70\ n_a < n_{\rm sj} < 1.15\ n_{\rm a}$, where the lower and upper limits also correspond to the quoted limits to $\Gamma_{\rm sj}$. In the ambient frame the shocked-jet density should be $1.08\ n_{\rm a} < \gamma_{\rm cd} n_{\rm sj} < 1.76\ n_{\rm a}$. Formally this represents the total density of particles in the shocked-jet region.

In the simulation the speed of the trailing density jump is $\sim 0.56\ c$, which is in the predicted range $0.35 < \beta_{\rm ts} < 0.61$. A typical speed within the density-plateau region, $\sim 0.75\ c$, is close to $\beta_{\rm cd} = 0.76$. The poorly defined leading shock structure moves at a speed between $\sim 0.76\ c$ and $\lesssim c$, consistent with the predicted $0.78 < \beta_{\rm ls} < 0.86$. The maximum density increase observed in the ambient (simulation) frame is $\gamma_{\rm cd} n_{\rm sa}/n_{\rm a} \sim 3.5$ behind the leading shock (see Fig. 1a). This is about a factor of ~ 3 smaller than the predicted increase, $8.2 < \gamma_{\rm cd} n_{\rm sa}/n_{\rm a} < 14.1$, for a fully-developed leading shock. On the other hand, the density increase observed in the ambient (simulation) frame of $\gamma_{\rm cd} n_{\rm sj}/n_{\rm a} \gtrsim 1$ just before the trailing large density jump is comparable to that predicted, $1.08 < \gamma_{\rm cd} n_{\rm sj}/n_{\rm a} < 1.76$, for a fully developed trailing shock.

Our present results can be compared to those found in the 2D simulations of Chang et al. ([3]) (see also [19]). Their simulations were performed in the CD frame, and material with proper density n moved into the contact discontinuity with Lorentz factor $\gamma = 15$. A shock moved away from the CD with the predicted speed

$$\beta_{\rm s} = (\Gamma_{\rm s}-1)\left[\frac{\gamma-1}{\gamma+1}\right]^{1/2} = 0.47, \qquad (4)$$

and predicted density jump

$$\frac{n_{\rm s}}{\gamma n} = \frac{1}{\gamma}\frac{\Gamma_{\rm s}\gamma+1}{\Gamma_{\rm s}-1} = 3.13, \qquad (5)$$

for a shocked adiabatic index for 2.5D gas of $\Gamma_{\rm s} = 3/2$.

In our simulation we have two shocks that move away from the CD. For our leading shock, the ambient plasma moves relative to the CD at a speed equal to $\beta_{\rm cd} = 0.759$ and $\gamma = \gamma_{\rm cd} = 1.54$ in (4) & (5). In the CD frame $\beta_{\rm s} = 0.23$ and the observed density jump becomes $n_{\rm sa}/\gamma_{\rm cd} n_a = 4.3$ for $\Gamma_{\rm s} = 3/2$. So we see that our leading shock speed would be about 50% less than that in [3] and our density increase would be about 50% larger for a fully-developed leading shock in the CD frame. For the trailing shock, the jet moves toward the CD at a speed equal to $-\beta'_{\rm cd} = 0.984$ and $\gamma = \gamma'_{\rm cd} = 5.60$ in (4) & (5), where $\beta'_{\rm cd} = -(\beta_{\rm j}-\beta_{\rm cd})/(1-\beta_{\rm j}\beta_{\rm cd})$ is given in the jet rest frame. In the CD frame $\beta_{\rm s} = 0.417$ and the observed density increase becomes $n_{sj}/\gamma'_{\rm cd} n_j = 3.36$ for $\Gamma_{\rm s} = 3/2$. So we see that our trailing shock speed would be about 11% less than that in [3] and our density increase would be about 7% larger for the fully developed trailing shock in the CD frame. The parameters associated with our trailing shock are thus similar to those found in [3], and the Weibel filamentation structures are comparable but now studied in full 3D.

V. Conclusion

The present simulation finds for the first time a relativistic shock system comparable to a predicted relativistic HD shock system consisting of leading and trailing shocks separated by a contact discontinuity, albeit not

yet fully developed. One remarkable aspect of this shock system lies in the generation of large electromagnetic fields, up to 30% of the kinetic energy density, associated with the trailing shock. Electromagnetic fields in the leading shock and contact-discontinuity region are over one order of magnitude lower. The large value for $\epsilon_B \sim 0.3$ in our trailing shock hints that Poynting-flux-dominated ejecta may not be required to explain some GRB observations ([7]).

Visualization of our dual-shock system in the ambient (simulation) frame provides a picture of the shock structure that should exist at the head of a relativistic astrophysical jet, moving with Lorentz factor $\gamma_{\rm jt} = 15$, that is less dense than the surrounding medium, $n_{\rm jt}/n_{\rm am} = 0.045$. Within the AGN context, here we identify our trailing shock with the "jet" shock that decelerates the relativistic jet and we would expect synchrotron emission to originate from the strongly magnetized structure. Little synchrotron emission would originate from the weakly magnetized "bow" shock in front of the contact discontinuity. This in fact is what is observed at the leading edge of extra-galactic jets where synchrotron emission from the bow shock is typically not observed.

Visualization of our dual-shock system in the "jet" frame provides a picture of the shock structure that would accompany a relativistic blast wave driven by relativistic ejecta. Within the GRB context, here we identify the ambient medium as representing relativistic ejecta moving at $\gamma_{\rm ej} = 15$ into a much less dense ISM, $n_{\rm ej}/n_{\rm ism} = 22$. Our trailing shock is now identified with the "forward" shock and we would expect synchrotron emission from this strongly magnetized structure. Little synchrotron emission would originate from the low Lorentz factor, weakly-magnetized "reverse" shock moving back into the ejecta.

Two-dimensional simulations of the system using much larger computational grids are now being performed. They enable us to find a fully-developed quasi-stationary relativistic shock system which can be compared to the HD model predictions. The HD picture assumes that the contact discontinuity separates the ambient and jet plasmas, and that the net flow across the CD should vanish (cf. our 3D simulation). The motion of the leading and trailing shocks is then driven and maintained by the interaction of the plasma reflected from the shocks with the streams of incoming matter. 2.5D simulations will allow us to fully resolve the formation of a dual-shock system and to investigate the structure of the self-generated electromagnetic fields and accompanying particle acceleration processes. The results of these simulations will be presented at the Conference and published elsewhere.

Our present simulations involve an electron-positron jet and ambient medium. We might expect similar shock-structure development in electron-ion simulations, albeit on much longer temporal and spatial scales. This is left to future studies with 2.5D simulations.

ACKNOWLEDGMENT

This work is supported by AST-0506719, AST-0506666, NASA-NNG05GK73G, NNX07AJ88G, NNX08AG83G, NNX08AL39G, and NNX09AD16G. JN is supported by MNiSW research project N N203 393034, and The Foundation for Polish Science through the HOMING program, which is supported by a grant from Iceland, Liechtenstein, and Norway through the EEA Financial Mechanism. Simulations were performed at the Columbia facility at the NASA Advanced Supercomputing (NAS) and Cobalt at the National Center for Supercomputing Applications (NCSA) which is supported by the NSF.

REFERENCES

[1] Blandford, R.D. & McKee, C.F. 1976, Phys. Fluids, 19, 1130
[2] Buneman, O., 1993, *Tristan*, in Computer Space Plasma Physics: Simulation Techniques and Software, edited by H. Matsumoto Matsumoto & Y. Omura, p. 67, Terra Scientific Publishing Company, Tokyo
[3] Chang, P., Spitkovsky, A., & Arons, J. 2008, ApJ, 674, 378
[4] Dieckmann, M.E., Shukla, P K. & Drury, L.O.C. 2008, ApJ, 675, 586
[5] Frederiksen, J.T., Hededal, C.B., Haugbølle, T., & Nordlund, Å. 2004, ApJ, 608, L13
[6] Jaroschek, C.H., Lesch, H., & Treumann, R.A. 2005, ApJ, 618, 822
[7] McMahon, E., Kumar, P., & Piran, T. 2006, MNRAS, 366, 575
[8] Medvedev, M.V. & Loeb, A. 1999, ApJ, 526, 697
[9] Medvedev, M.V. & Zakutnyaya, O.V. 2009, ApJ, 696, 2269
[10] Mizuno, Y., Zhang, B., Giacomazzo, B., Nishikawa, K.-I., Hardee, P., Nagataki, S., & Hartmann, D.H., 2009, ApJ, 690, 47L
[11] Niemiec, J., Pohl, M., Stroman, T. & Nishikawa, K.-I. 2008, ApJ, 684, 1174
[12] Nishikawa, K.-I., Hardee, P., Richardson, G., Preece, R., Sol, H., & Fishman, G.J. 2003, ApJ, 595, 555
[13] Nishikawa, K.-I., Hardee, P., Richardson, G., Preece, R., Sol, H., & Fishman, G.J. 2005, ApJ, 622, 927
[14] Nishikawa, K.-I., Hardee, P., Hededal, C.B., & Fishman, G.J. 2006, ApJ, 642, 1267
[15] Nishikawa, K.-I., Niemiec, J., Hardee, P., Medvedev, M.V., Sol, Mizuno, Y., Zhang, B., Pohl, M., Oka, M., & Hartmann, D.H., 2009, ApJL, accepted, (arXiv:0904.0096)
[16] Ramirez-Ruiz, E., Nishikawa, K.-I., & Hededal, C.B., 2007, ApJ, 671, 1877
[17] Rosen, A., Hughes, P.A., Duncan, G.C., Hardee, P.E., 1999, ApJ, 516, 729
[18] Silva, L.O., Fonseca, R.A., Tonge, J.W., Dawson, J.M., Mori, W.B., & Medvedev, M.V., 2003, ApJ, 596, L121
[19] Spitkovsky, A. 2008a, ApJ, 673, L39
[20] Spitkovsky, A. 2008b, ApJ, 682, L5
[21] Weibel, E.S. 1959, Phys. Rev. Lett., 2, 83
[22] Zhang, B. & Kobayashi, S. 2005, ApJ, 628, 315